Available online at www.sciencedirect.com
SCIENCE DIRECT®
International Journal of Multiphase Flow 31 (2005) 115–140
International Journal of Multiphase Flow
www.elsevier.com/locate/ijmulflow

The liquid deposition fraction of sprays impinging vertical walls and flowing films

C. Weiss

Institute of Process Technology and Industrial Environmental Protection, University of Leoben, Peter-Tunner Straße 15, A-8700 Leoben, Austria

Received 19 February 2003; received in revised form 2 August 2004

Abstract

The impingement of coarse sprays with a mean diameter in the order of millimeters on vertical walls with and without an additionally supplied wall film was studied at conditions well below the Leidenfrost limit. The fraction of the sprayed liquid deposited on the wall was determined experimentally and theoretically for various impingement angles with the help of a flat fan spray directed against the wall. The deposition fraction shows a distinct minimum in the range of intermediate impingement angles. This fact cannot be described by single-droplet-based deposition-splash criteria when considering the droplet's impact momentum alone. The investigation demonstrates that the measurement results can be explained by including the collision of splashed droplets with incoming ones. In principle, the entrainment of the primary spray's fine fraction in the gas flow field may also be of relevance. For the coarse and relatively sparse sprays investigated, the importance of the collisions in determining the overall balance of deposited and splashed liquid was estimated by event statistics derived from Monte Carlo simulations. The main outcome of wall interaction for the coarse spray is splashing. The splashed droplets form a secondary spray. When the impingement angle is steep, the splashed liquid is redirected towards the wall as a result of the collision between the incoming primary spray and splashed droplets.

Keywords: Spray/wall interaction; Spray impingement angle; Liquid deposition; Splash criterion; Inter-droplet collision

0301-9322/$ - see front matter © 2004 Elsevier Ltd. All rights reserved.
doi:10.1016/j.ijmultiphaseflow.2004.08.004

1. Introduction

In the spray/wall impingement, the main variables of interest are the fraction of liquid deposited on the wall and the fraction which rebounds or "splashes" in a re-dispersion process to form a secondary spray. The rebound of droplets at the solid surface or at the wall film is restricted to the low impact-momentum regime. The re-dispersion process is initialized by the formation and break-up of the impact lamella and produces secondary spray droplets by splashing. Droplet impact has recently been reviewed by Rein (1993), Prosperetti and Oguz (1993) and Tropea (1999). Droplet deposition and splashing were among others investigated by Mundo et al. (1995) for single droplet impact on dry walls, by Walzel (1980), Reske (1987) and Coghe et al. (1995) for single droplets impacting thin films, by Macklin and Metaxas (1976) for impact into deep or shallow liquids and by Samenfink et al. (1997) for droplets impacting on gas shear-driven liquid films.

The amount of liquid deposited on walls is of considerable importance in practical applications such as combustion engines, spray cooling and coating. Gas streams are contacted by sprays in gas absorption, in the reduction of dust emissions or in chemical reaction engineering. In spray tower design, it is of interest to minimize the amount of the spray's interfacial area, which is lost by wall deposition. Thereby an analysis of droplet deposition and splashing on wetted walls and flowing liquid films is considered to be useful.

Few measurements are reported on the split of the spray flux into the deposited and splashed liquid fractions. Results for the secondary droplets' mass flux are reported by Yarin and Weiss (1995). Sophisticated measurements were performed by Samenfink et al. (1997) for monosized droplet chains impacting shear driven liquid films. Tropea and Roisman (2001) measured the depositing flux of impinging sprays. For single droplet impact models they realized a deficiency in the predicted amount of deposition. Discrepancies were attributed to droplet collisions, crown interaction and wall film fluctuations. For coarse flat fan sprays impacting various wall materials, deposition fractions have been quantified by Wieltsch et al. (1998). In the present investigation, spray deposition fractions on scrubber wall materials are determined experimentally for coarse sprays, which are typical in flue-gas scrubbing applications with droplet Reynolds numbers and Ohnesorge numbers covering a broad range within $10 < Re < 5 \times 10^5$ and $10^{-3} < Oh < 10^{-1}$. Splash criteria considering single droplet impact events alone will be demonstrated to be insufficient to predict the magnitude of the deposition fraction in the poly-disperse spray. Literature reports splash models which match, overestimate or underestimate the experimentally determined deposition fraction, particularly for low impact angles, with respect to primary spray jets directed nearly tangentially towards the wall. These findings suggest the action of a competing mechanism, which might suppress an increased splashing intensity in the range of the maximal impact momentum for nearly normal directed spray inclinations. Within the further analysis the inter-droplet collision between splashed and primary spray droplets turns out to be a potential candidate for the proposed competing mechanism.

In the outcome of droplet–droplet collisions, a number of possible scenarios are known. In the case of *coalescence* the droplets will merge and form a stable product droplet. In case of a non-central collision, the temporarily coalesced droplet pair may not be able to dissipate the kinetic energy of the impact and may split in a kind of ligament break-up process, which is termed *stretching separation*. O'Rourke and Bracco (1980) referred to this mechanism as 'grazing collision'. The boundary between coalescence and stretching separation was recently investigated in

detailed experiments by Brenn et al. (1997), Brenn et al. (2001) and Blei and Sommerfeld (2002). Even in the case of pure 'head on' collisions the merged liquid might split up again: Under the action of capillary forces the flattened disc formed after the impact changes shape into a cylinder, which is stretched due to inertial forces. Thereafter, droplets moving in opposite directions are produced by ligament breakup. This mechanism produces what was called *reflexive separation* and was explored by Ashgriz and Poo (1990). During the gas film drainage prior to merging an additional phenomenon, *bounce*, is described by Estrade et al. (1999); however, it is not observed for water droplets at atmospheric pressure.

The wall-jet configuration of impinging (fuel) sprays was recently visualized experimentally among others, by Mohammadi et al. (2000). The gas co-flow with the spray towards the wall generates a stagnation zone where the incoming gas is deflected from its freestream direction into a wall-jet, moving away from the impingement location. The primary spray fine-fraction containing droplets with sufficiently small relaxation time may partly follow the gas streamline curvature in the jet-deflection region and thereby will escape the impact by entrainment within the wall-jet. In principle the entrainment fraction can be quantified by a critical droplet's Stokes number, defined in analogy to Marple's impact theory; Marple and Liu (1974). A rough estimation shows the upper limit of potentially entrainment-affected droplet sizes in the investigated spray lies in the order of 50–100 μm. The volumetric fraction of these droplets is negligibly small in the sprays and therefore an entrainment fraction will not be further considered in the overall liquid flux balance.

The aim of the present study is to validate and further develop the 'competing mechanism' hypothesis by experimental and theoretical means. The liquid deposition on the wall is investigated experimentally in Section 2. Selected deposition-splash criteria are compared in Section 3.1. In Section 3.2 the potential of inter-droplet collisions to account for the deviation of the spray results from the single droplet based deposition predictions are analyzed. In Section 4 the quantitative significance of the theoretically predicted deposited and splashed liquid fractions are demonstrated by Monte Carlo simulations, which take into account the outcome of inter-droplet collision.

2. Experimental investigation of a flat fan spray

2.1. Measurement techniques

Due to its similarity to a circumferential segment of a hollow cone spray and to draw advantages from a simple geometrical configuration, a flat fan spray was chosen for the experiments. For a given liquid ejection pressure, the droplet impact momentum can be varied by the spray inclination angle against the wall, while keeping the distance L of the nozzle to the impact location constant; see Fig. 1. Thereby the wall normal component of the droplet momentum will increase from a marginal value for flat impact angles up to the maximum at the spray directed normal to the wall. Due to increased splashing intensity in the case of steeper impact angles, the deposition fraction is expected to decrease correspondingly.

In the experiments a flat fan spray nozzle (Spraying Systems, 1/2 P 3580) was operated at liquid ejection pressures of $\Delta p = 0.3$, 0.5 and 0.7 bar. The angular ejected mass flux in $[\mathrm{m^3\,deg^{-1}\,s^{-1}}]$ is in the order of the feed stream of the conical liquid sheet in typical spray tower nozzles for gas

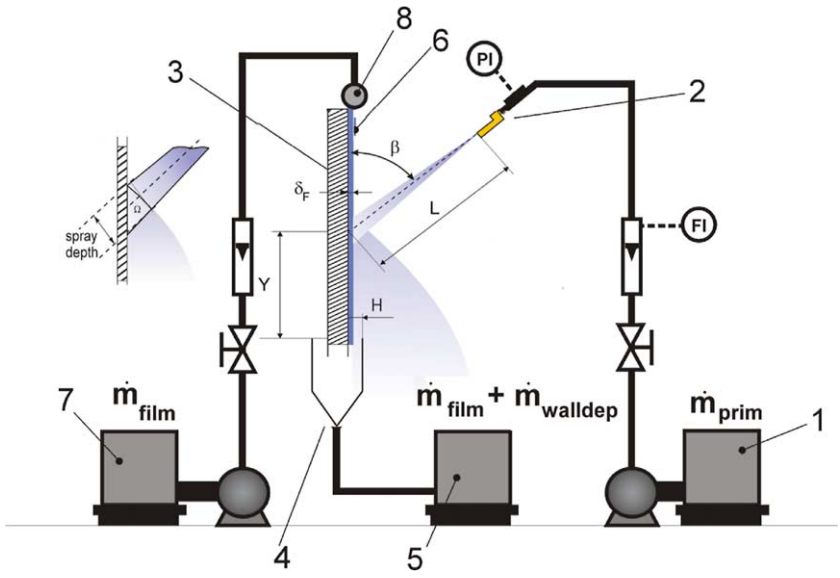

Fig. 1. Experimental set-up to determine the deposition fraction during spray impingement.

scrubbing applications. Measurements were performed in three steps: (1) characterization of the primary spray; (2) determination of the amount of water deposited at the wall as a function of ejection pressure, impingement angle, wall material and wall film; (3) measurement of the size and velocity distribution of the secondary spray.

The impinging primary and secondary spray flows are characterized by the phase Doppler technique with a DANTEC 2D-LDA, 1-D PDPA system operated with a COHERENT 10 W argon ion laser. Table 1 summarizes the optical parameters of the instrumentation. Within the flat spray jet, measurements were performed at a distance of 0.5 m downstream from the nozzle exit at nine discrete, equally spaced positions in the cross-section. The local spray flux density was constant except for the outermost points and the data was averaged over the remaining central measurement positions. Table 2 summarizes the primary spray results. In the secondary spray, data was taken at levels 150 and 450 mm below the point of impingement. The first measurement location was 5 mm away from the wall and further points followed at equal spacings of 10 mm. Since it is not practical to change the LDA-PDPA adjustment during the experiments, the plate and nozzle were moved relative to the instrument.

The amount of water deposited was determined for typical wall materials used in flue gas scrubbers: stainless steel (polished), Kerabutyl V, Kerabutyl BS and Ceilcote 140 Flakeline (all three

Table 1
Specifications of the LDA/PDA measurement system

Laser wavelength	514.5 and 488 nm	Angle of intersection	2.2°
Laser power	300 and 600 mW	Number of fringes	29
Beam diameter	1.7 mm	Fringe spacing	13.4 μm
Beam separation	28.4 mm	Measurement volume	$0.39 * 0.39 * 20.1$ mm
Focal length of LDA receiver	1000 mm	Focal length of PDA reciever	1000 mm

Table 2
Spray characteristics of the investigated flat fan spray nozzle

Ejection pressure [bar]/throughput [m^3/h]	Mean droplet velocity [m/s]	Mean droplet diameter d_{10} [μm]	Sauter mean diameter d_{32} [μm]
0.3/0.600	5.2	228	813
0.5/0.775	7.1	219	823
0.7/0.915	8.3	221	810

products from SGL Carbon Group, Germany). The deposition fraction as a function of the impingement angle showed noticeable differences due to material-specific wettability and surface roughness; cf. Wieltsch et al. (1998). In the current context the spray impingement on Kerabutyl V is analyzed in detail. The experiments were carried out both with and without an additional film flow smoothly running down the wall. The film thickness was maintained within 0.45 and 0.55 mm. The deposition rate was determined as follows (see Fig. 1). The nozzle (2) is fed from the tank (1). The spray is directed against plate (3) with the impingement angle varied between 15° and 75°. To keep the spray's flight distance constant ($L = 0.5$ m) during the impingement angle variation, the nozzle inclination is changed together with the nozzle position by a traversing mechanism. The deposited water is collected by a receiver (4) and is stored in run-down tank (5). The additional wall film (6) is produced by the wall film generator (8) connected to the feed tank (7). The valves, flowmeters and manometers control the experiment. The deposition rate followed from a simple mass balance and therefore the tanks stood on scales.

2.2. Characterization of the primary spray

The characteristics of the flat fan spray, produced from a single-orifice pressure nozzle, as used in our experiments were investigated intensively by Dombrowsky and co-workers; see Briffa and Dombrowski (1966) and the references cited therein. The liquid issuing from the nozzle is transformed into a liquid sheet which is subject to aerodynamic and pressure forces. The lateral width of the sheet is determined by the extent to which the edges of the liquid layer have contracted due to surface tension. Growing waves break-up the sheet into fragments, which rapidly disintegrate further into droplets. The break-up length of the sheet shows a slight dependence on the ejection pressure and was in the order of some centimeters for the pressure range investigated. The spray angle was approximately 26°. The finite spray depth of the flat fan spray is a result of the droplet velocity component normal to the sheet, which is induced by the wave motion in the moment of break-up. At a distance of 0.5 m downstream from the nozzle, the spray depth reaches approximately 20 mm. As pointed out by Briffa and Dombrowski (1966), the spray depth becomes more pronounced with increased ejection pressure.

The cumulative number distribution plot of the primary spray can be described by

$$q_0(d) = \frac{c}{\sigma_{\ln}(\sqrt{2\pi})d} \exp[0.5 \ln(d/d_{n0.5})/\sigma_{\ln}], \tag{1}$$

which is a log-normal distribution with a fitting parameter c and a median value $d_{n0.5}$ of the droplet number distribution. The standard deviation of $\ln(d)$ is denoted by $\sigma_{\ln}$, which is estimated from $\sigma_{\ln} = \ln(d_{n0.84}/d_{n0.5})$. The measured size distributions are independent of the ejection pressure

within the range of 0.3–0.7 bar and are described by Eq. (1) with the distribution parameters $c = 10.1$, $\sigma_{\ln} = 1.340$, $d_{n0.5} = 110\,\mu m$.

A size cut-off introduced in the raw data processing excluded droplets with $d_{prim} > 2\,mm$. Thereby a contamination of the size spectra by large, potentially non-spherical droplets should be avoided. The "lost" cut-off volume was estimated by a liquid mass balance to be smaller than 4% for all investigated ejection pressures. A diagram of *Oh*- versus *Re*-number of the primary spray is shown in Fig. 2. Note that as a consequence of the coarse-sized spray, the droplet-fraction to the right of the solid line marking the single-droplet-based splashing deposition limit $K_{cr} = Oh\,Re^{1.25} = 138$ contains approximately 90% of the liquid volume.

Fig. 3 shows the droplet mean velocity distribution as influenced by the ejection pressure and to a lesser extent by the droplet size. Only droplets <300 μm show a remarkable decrease of mean droplet velocity due to the relaxation of the droplet injection velocity induced by the action of

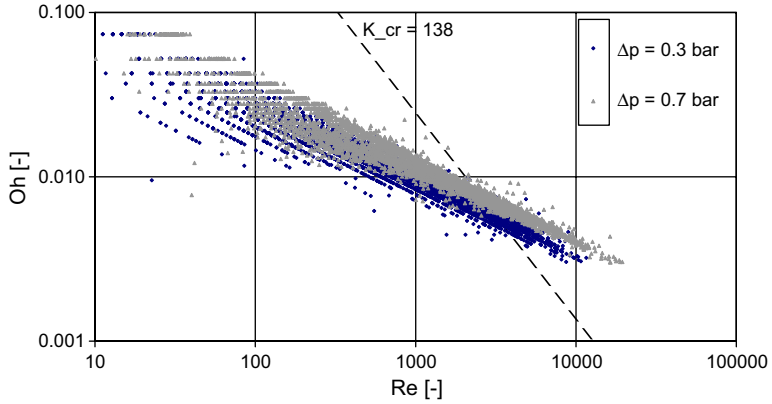

Fig. 2. *Oh–Re* plot of the primary spray; liquid ejection pressure is 0.7 bar and 0.3 bar; the measurement point is 0.5 m downstream from the nozzle.

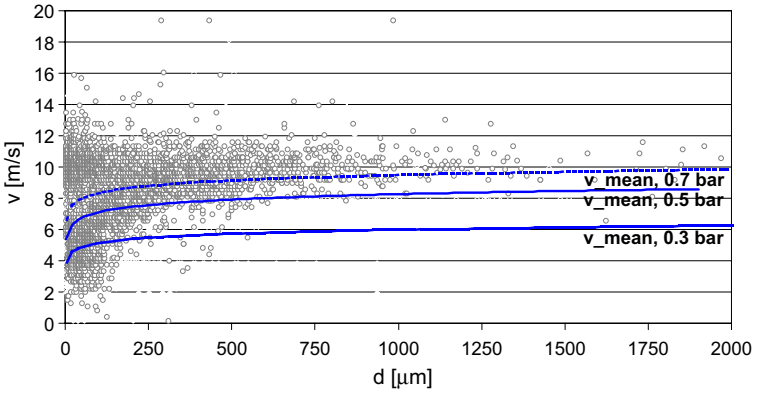

Fig. 3. Primary spray: size specific axial component of the droplet velocity for different liquid ejection pressures; data points of experiment with ejection pressure $\Delta p = 0.7$ bar.

the aerodynamic drag along the flight distance. However, the droplet's velocity fluctuation is shown by the velocity-size correlation to increase strongly with decreasing droplet size. For droplet sizes <300 μm the averaged droplet velocity fluctuation within the size classes reaches a level in the order of the droplet mean velocity.

2.3. Results and discussion of the liquid deposition fraction measurements

Fig. 4 shows the deposition rate on Kerabutyl V with and without an additional wall film. The experimental series for all materials produced trends with several common features. Minima of the deposition fraction can be found in the range $40° < \beta_{min} < 60°$. The exact angle β_{min} of the deposition minimum depends on the ejection pressure and the presence of a wall film. In the experiments with a wall film the spray deposition tends to be lower as compared to the cases without a film. Note furthermore, that each set of curves shows a distinct 'crossover'-point, where the influence of the nozzle feed pressure changes its trend: A higher pressure reduces the spray deposition for small impingement angles and vice versa.

Within the branch $15° < \beta < \beta_{min}$ only a minor interaction between primary and secondary spray is expected. Thereby the deposition fraction is mainly a result of single droplet impact dynamics. The increase of the deposition fraction reflects the fact that small impingement angles against the wall will reduce the number of droplets exceeding a critical impact momentum. A steeper impingement angle will increase the number of droplets with a critical impact momentum for splashing and therefore increase the splashed liquid fraction. The same argument explains the reduced deposition for higher impact pressure on the left side of the 'crossover'-point for both curve sets in Fig. 4. Within the branch $\beta_{min} < \beta < 75°$ a strong interaction of the primary and secondary spray is expected. The splashed liquid is partially redirected towards the wall by collision intensity between incoming primary droplets and the secondary spray. This mechanism will increase the deposition fraction.

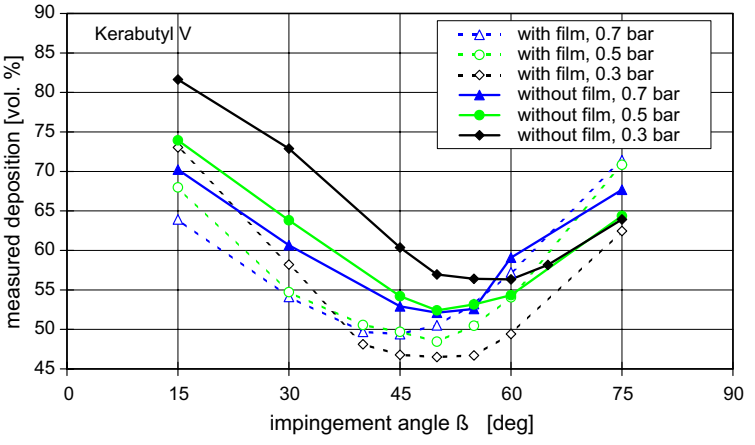

Fig. 4. Deposition rate versus impingement angle for different ejection pressures at Kerabutyl V; with and without an additional wall film.

Further details in Fig. 4 support the existence of the proposed regime of enhanced droplet interaction. Starting from the 'crossover' of the curve sets, the deposition fraction increases with increasing ejection pressure according to the increased impact velocity. These findings are consistent with the fact that the collision frequency ν_{coll} will be proportional to the relative velocity u_{rel} between the primary and the splashed droplets; (this reasoning is detailed further in the modelling). Note, that in the case of the experiments with wall film the 'crossover'-point of the ejection pressure influence as well as the deposition minimum at β_{min} are reached at a less steep impact angle. For the spray impingement with an additional wall film, both facts indicate an increased range of spray inclination whereby the resulting liquid deposition is influenced or even dominated by the droplet interaction mechanism.

Within the 'single droplet impact' branch ($\beta < \beta_{min}$) the resulting deposition fraction is lower if a wall film is present; see Fig. 4. An additional wall film promotes the formation of a steeper impact lamella, Macklin and Metaxas (1976). Thereby the splashed droplets tend to be ejected from the wall with a decreased tangential component. This observation is consistent with the measured secondary droplet tangential velocities in Fig. 8 and will increase the splashed droplets residence time within the interaction domain of the primary and secondary sprays. Within the 'enhanced droplet interaction' branch ($\beta > \beta_{min}$) the collision intensity is therefore expected to be increased by the presence of the film.

2.4. Characterization of the secondary spray

The secondary spray's arithmetic mean diameter d_{10} as calculated from the averaged contributions of the measurement positions 150 mm below the impact location is shown in Fig. 5. With increasing impact pressure the droplet sizes are slightly reduced in comparison to the primary spray. For a given ejection pressure the cases with additional wall film always produce a slightly coarser secondary spray. With the exception of the 0.3 bar data series with a wall film (which shows minor deviations) the mean droplet size does not change significantly for different impingement angles. Contrary to the relatively uneffected d_{10} the Sauter diameter d_{32} of the secondary spray is increased in the order of 25% by addition of a wall film.

Fig. 6 shows the size distributions of the primary and the secondary sprays at impingement angles of 15°, 45° and 75°. The size distributions of the secondary spray are centred nearly at the same position on the size axis. However, their spread is considerably smaller than that of the primary spray. The coarser size fraction of the primary spray, $d_{prim} \gtrsim 1000\,\mu m$, is reduced by splashing and interaction effects. Thereby a fresh droplet population in the size range of $300 \lesssim d_{prim} \lesssim 1000\,\mu m$ is produced, which is clearly visible by the increased steepness of the secondary spray size distribution curves within this range as compared that of the primary spray. Fig. 6 reveals that the fine fraction of the primary spray, $d_i \lesssim 300\,\mu m$, is strongly reduced during impingement, which is probably due to deposition of the fine fraction on the wall or film. A comparison of the secondary spray at 150 mm and 450 mm below the impact location (not shown in Fig. 6) demonstrated the progressive decrease of the fine fraction along the downstream spray path. This reduction might be caused by the continuous deposition of the small droplets on the wall or on the coarse droplet fraction.

Fig. 7 shows the cumulative number distribution of the secondary spray for measurement locations at various normal distances from the wall. With increasing distance from the wall the fine

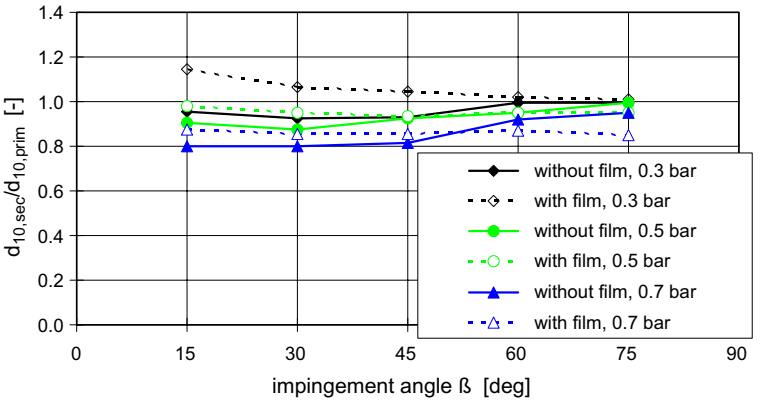

Fig. 5. Impingement angle dependence of the secondary spray mean diameter for different ejection pressures; measurements at a level of $z = -150$ mm below the impact location.

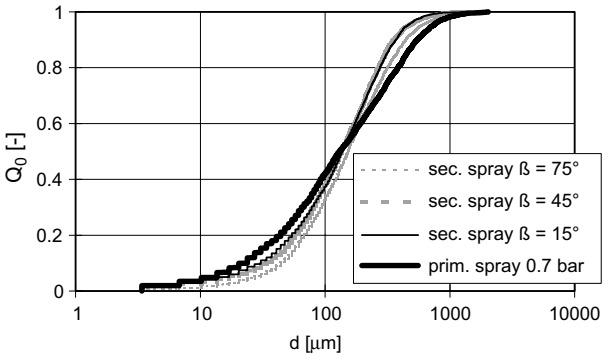

Fig. 6. Droplet size distribution of the primary spray and the secondary sprays at 0.7 bar; measurement location $y = 25$ mm, $z = -150$ mm, additional wall-film present.

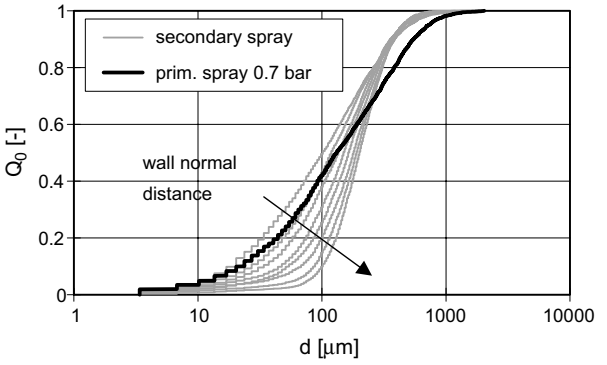

Fig. 7. Cumulative number distribution of droplet sizes in the secondary spray as a function of the wall normal distance; $x = 5$ mm up to 75 mm, stepsize 10 mm; ejection pressure $\Delta p = 0.7$ bar, measurement level $z = -150$ mm, impingement angle $\beta = 45°$, additional wall film.

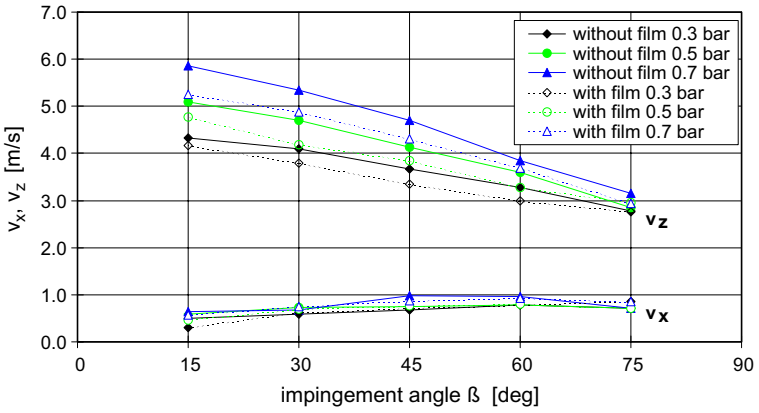

Fig. 8. Wall tangential and normal components of the droplet velocity in the secondary spray; ensemble average of data at all measurement positions at a level of $z = -150$ mm.

fraction in the secondary spray is continuously reduced. A considerable amount of droplets smaller than 50 μm are present only in the near-wall region. The droplets are transported away from the impingement location due to the entrainment within the primary spray induced wall-jet. The coarse fraction of the splash products with droplet sizes in the range $300 \lesssim d_{\text{sec}} \lesssim 1000$ μm is not effected by the entrainment action, as can be deduced from the nearly identical shape of the distribution functions within this size range.

The mean values of the droplet velocity components tangential and normal to the wall are summarized in Fig. 8. The wall tangential component v_z increases with rising ejection pressure and, as already mentioned, decreases with the presence of a wall film. It is reduced almost linearly for steeper impingement angles due to the lower tangential momentum provided by the primary spray. The influence of the ejection pressure and the wall film diminishes with steeper impingement angles, which might also be caused by the dominating effect of droplet interactions on the secondary spray characteristics. The mean normal velocity v_x is relatively constant for all investigated impingement angles and injection conditions. Consequently the secondary spray leaves the wall with a remarkably flat secondary spray angle. At the level $z = -150$ mm the mean secondary spray angle is 6° from the wall in the flat impingement configuration ($\beta = 15°$) and increases slightly to 12° from the wall with steep impingement ($\beta = 75°$). The range of dominating secondary spray injection angles corresponds to droplet absolute velocities within the limits of $2.8 < |\vec{v}_{\text{sec}}| < 5.9$ m/s for the experiment without wall film and within $2.8 < |\vec{v}_{\text{sec}}| < 5.2$ m/s in the case with a wall film.

3. The modeling of physical mechanisms accompanying spray/wall interaction

3.1. Comparison of splash models based on single droplet impact mechanisms

The experimental findings concerning the liquid deposition fraction will be compared with predictions of models based on single droplet deposition/splash criteria for different primary spray

impingement angles. The underlying and strongly simplifying assumption is that the outcome of the spray impingement can be described as a superposition of single droplet impact mechanics.

Mundo et al. (1995) formulated a hypothesis for the regime discrimination based on the impact momentum threshold in terms of a non-dimensional critical K number as

$$K = Oh\,Re^{1.25}, \tag{2}$$

where Oh is the Ohnesorge number $Oh = \mu/(\rho\sigma d_{\mathrm{prim}})^{1/2}$ and Re is the Reynolds number based on the droplet's velocity component normal to the wall, $Re = \rho v_x d_{\mathrm{prim}}/\mu$. Herein μ is the dynamic viscosity of the liquid, and ρ its density. The surface tension is denoted by σ and d_{prim} is the incoming droplet's diameter. In the notation, the symbol v denotes absolute droplet velocities with the wall normal and tangential components v_x and v_z, the symbol u will be used in definitions of relative velocities between droplets and the symbol w_{g} will be reserved for the gas phase velocity.

For dry and smooth walls Mundo et al. (1995) determined a value of $K_{\mathrm{cr}} = 57.7$. If a wall film of mean thickness δ is present, the first occurrence of splashing is shifted to higher values of K_{cr}, as it had been shown in the experiments of Cossali et al. (1997), where a value of $K_{\mathrm{cr}} = 138$ was suggested. For the special case of water ($Oh = 0.0022$) as the splashing liquid this limit turned out to be independent of the film thickness when considering a dimensionless film thickness $\delta_{\mathrm{f}} = \delta/d_{\mathrm{prim}} > 0.2$.

From a number of alternative formulations two further splash criteria will be considered in the comparison. Coghe et al. (1995) took into account the dependence on film thickness explicitly in compiling their data for impact on liquid films by

$$We_{\mathrm{imp}}\,La^{0.2} \geqslant 1900 + 6240\delta_{\mathrm{f}}^{1.4}. \tag{3}$$

Therein the wall impact Weber number is defined by $We_{\mathrm{imp}} = \rho v_x^2 d_{\mathrm{prim}}/\sigma$ and the Laplace number is $La = \rho\sigma d_{\mathrm{prim}}/\mu^2$. The significance of this splash criterion was also discussed in the experimental analysis of Brenn et al. (1996). If the left side of Eq. (3) is larger than the right side, the generation of secondary droplets by splashing of the incoming droplet is predicted.

O'Rourke and Amsden (2000) extended the dry wall splashing criterion of Mundo, Eq. (2) to cover the droplet impact on wetted walls. They introduced an impact parameter E based on a splash Mach number, which was mentioned by Yarin and Weiss (1995) as a ratio of the droplet impact velocity to the capillary wave speed of a wave with wavelength $\lambda = d_{\mathrm{prim}}$ in the film. O'Rourke and Amsden (2000) applied this Mach number definition to non-dimensionalize the normal component of the droplet impact velocity by

$$E = v_x\left(1/d_{\mathrm{prim}}\sqrt{\sigma\delta_{\mathrm{f}}/\rho}\right)^{-1}. \tag{4}$$

With a boundary layer thickness $\delta_{\mathrm{bl}} = d_{\mathrm{prim}}\,Re^{-0.5}$ inserted in (4) as the length scale instead of the film thickness δ_{f}, the criterion of Mundo et al. (1995) can be recovered by the equality $E = K$. To avoid a division by zero in case of vanishing film thickness, the sum of film thickness and the boundary layer thickness is introduced in the inequality $\widetilde{E} > E_{\mathrm{crit}}$ with

$$\widetilde{E}^2 = We_{\mathrm{imp}}\frac{1}{\min(\delta_{\mathrm{f}}/d_{\mathrm{prim}}, 1) + \delta_{\mathrm{bl}}/d_{\mathrm{prim}}} > (57.7)^2. \tag{5}$$

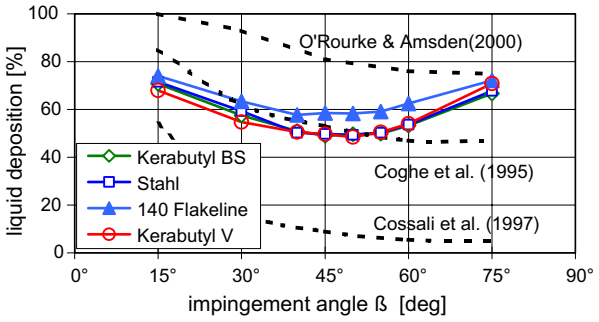

Fig. 9. Single droplet impact model predictions versus experimental data for the wall deposition fraction as a function of the impingement angle; flat fan spray nozzle, liquid feed $V_l = 2.15\text{e}{-4}\,\text{m}^3/\text{s}$ at $\Delta p = 0.5\,\text{bar}$, spray path length $L = 0.5\,\text{m}$, no additional wall film.

The increase of the film thickness beyond the value of d_{prim} is considered as ineffective for the splash event. The criterion (5) reflects the damping of the splash by the presence of the film, which will increase the dissipation of impact energy during the re-dispersion process of the spray. Furthermore, energy might be radiated away from the impact site by capillary waves.

In the comparison the deposition/splash criteria are applied on all primary spray droplets approaching the wall. The total liquid deposition fraction is estimated, assuming in the case of splashing, that the splashed mass and the mass of the impacting droplet are conserved. No empirical expression for the deposited volume fraction of a single droplet as a function of impact parameters is used. All primary spray droplets are considered individually and potential interaction effects between the droplets and the splashing lamella of adjacent impact sites are neglected. In Fig. 9 the model predictions are compared with experimental data of the liquid deposition fraction for the flat fan spray. The normal component of the impinging spray droplet velocities and the droplet diameters, as extracted from the PDA-data of the primary spray, were used as input to evaluate the splash models. The comparison includes the splash criterion (2) with $K_{\text{cr}} = 138$ according to Cossali et al. (1997), Eq. (3) according to Coghe et al. (1995) and Eq. (5) according to O'Rourke and Amsden (2000). To enable application of these models in the general case of non-perpendicular spray impact, the normal velocity component of the incoming droplet was used to quantify the impact momentum.

As demonstrated in the experimental section, the measured deposition fraction lays within the limits of 55–70% over the investigated range of impact angles. The model predictions are spread over a wide range of deposition fractions and typically show a decreasing trend for steeper impact angles, whereas the experiments demonstrate the existence of a minimum of the deposition to be located in the intermediate impact angle range, between 45° and 55°. As a consequence, the physical mechanism modeled by the single droplet based splash criteria alone turns out to be insufficient to predict the magnitude of the deposition fraction in the poly-disperse spray.

3.2. Inter-droplet collision

Droplet–droplet collision is expected to influence the spray deposition in the near wall region for several reasons. The droplet number concentration will increase near the wall due to the re-

duced velocity of splashed droplets and to a lesser extent due to the deceleration of the fine fraction in the stagnation region of the impinging two-phase jet. The relative velocity between potential collision partners is high due to the counter-current or at least cross-current directed motion of the primary spray and the splashed droplets. The effective collision cross-section of a splashed droplet can exceed the diameter of its equal volume sphere, due to a possible droplet deformation during the splash process, which might not have been reshaped completely in a short time period after the ejection from the wall film.

A flow domain Ω can be defined to mark the region of enhanced droplet interaction intensity. The boundaries of the domain Ω are identified by the intersection of the volume covered by the primary spray jet with the enveloped volume of all possible splashed droplet trajectories; see Fig. 1. An estimate of the frequency ν_{coll} of collisions taking place between a splashed droplet and the primary spray droplets in the domain Ω can be derived according to the kinetic theory of gas:

$$\nu_{\mathrm{coll}} = A_{\mathrm{eff}} \mid \vec{u}_{\mathrm{rel}} \mid n_{\mathrm{d}} \approx \frac{\pi}{4}(d_{\mathrm{splash}} + d_{\mathrm{prim}})^2 \mid \vec{u}_{\mathrm{rel}} \mid n_{\mathrm{d}}. \tag{6}$$

The relative velocity between the primary and splashed droplets is denoted by $\vec{u}_{\mathrm{rel}} = \vec{v}_{\mathrm{splash}} - \vec{v}_{\mathrm{prim}}$ with the absolute velocities of the primary spray droplet $\vec{v}_{\mathrm{prim}}$ and an individual splashed droplet $\vec{v}_{\mathrm{splash}}$. The droplet number concentration of the primary spray jet within Ω is denoted by n_{d}. As demonstrated by Eq. (6), an increase of n_{d}, $\vec{u}_{\mathrm{rel}}$ and of the effective collision cross-section will lead to higher collision frequency of the primary spray and splashed droplets. On the right side of Eq. (6) the term in front of n_{d} is the volume covered per second during sweeping the effective collision cross-section along the splashed droplet path. The average number of collisions between the primary spray droplets and a single splashed droplet within Ω is given by

$$N_{\mathrm{coll}} = n_{\mathrm{d}} V_{\mathrm{eff}} = n_{\mathrm{d}} A_{\mathrm{eff}} \int_{t=0}^{\tau} \mid \vec{v}_{\mathrm{splashed}} - \vec{v}_{\mathrm{prim}} \mid \mathrm{d}t. \tag{7}$$

Note that due to the movement of the primary droplets, V_{eff} is larger than the geometrical swept volume V_{swept} along the trajectory path of length s within the interaction domain Ω, which would be $V_{\mathrm{swept}} = sA_{\mathrm{eff}}$. In Eq. (7) τ denotes the residence time of the splashed droplet within Ω. In the evaluation of Eq. (7) suitable average values for the primary and secondary spray properties, d_{prim}, $\vec{v}_{\mathrm{prim}}$ and d_{splash}, $\vec{v}_{\mathrm{splash}}$ must be defined. The colliding liquid mass flux $\dot{m}_{\mathrm{coll\_tot}}$ can be expressed from the average number of collisions within Ω, N_{coll}, and the splashed liquid mass flux $\dot{m}_{\mathrm{splash\_tot}}$

$$\dot{m}_{\mathrm{coll\_tot}}/\dot{m}_{\mathrm{splash\_tot}} = 1 - \exp(-N_{\mathrm{coll}}). \tag{8}$$

Following the standard approach the model of O'Rourke and Bracco (1980) is applied. It is based on the derivation of Brazier-Smith et al. (1972) to determine the outcome of a collision event according to its dimensionless characteristics (the Weber number We, the impact parameter B and the drop size ratio) as coalescence or as stretching separation. Further alternative mechanisms following a collision process are neglected in this analysis. The current implementation is similar to the one recently described by Gavaises et al. (1996) and Post and Abraham (2002). The nomenclature of Post and Abraham (2002) is applied in the following, with index 1 denoting

the smaller and index 2 the larger droplet's radius and absolute velocity prior to the collision. Deviating from their formalism, the Weber number is defined for the smaller droplet to maintain consistency with the original derivation of Brazier-Smith et al. (1972):

$$We = \rho \mid \vec{v}_1 - \vec{v}_2 \mid^2 r_1/\sigma. \tag{9}$$

The geometry of the collision configuration is summarized in the impact parameter B, defined as $B = b/(r_1 + r_2)$. Therein b denotes the displacement of the droplet centers, as seen along the direction of the relative velocity vector; according to Fig. 10b. The limiting value $B = 0$ defines a central collision and in case of $B = 1$ the droplets only slightly graze each other. The drop size ratio is defined as $\gamma = r_2/r_1$ and therefore $\gamma \geqslant 1$ is always fulfilled.

The displacement of each collision event is defined stochastically by $B = YY$ and therefore $b = YY(r_1 + r_2)$, where YY is a random number uniformly distributed in the range $(0,1)$. The result of a collision is classified to be coalescence as long as the displacement b is smaller than a critical value b_{cr}. Highly off-centre collisions are characterized by $b \geqslant b_{cr}$ and result in stretching separation. For the critical displacement of two impinging droplets the following correlation was given by Amsden et al. (1989):

$$b_{cr}^2 = (r_1 - r_2)^2 \min(1.0, 2.4 f(\gamma)/We); \quad f(\gamma) = \gamma^3 - 2.4\gamma^2 + 2.7\gamma. \tag{10}$$

The velocity after coalescence is calculated as the outcome of a total inelastic collision. For a reference system with the smaller droplet at rest, the relative velocity after the collision is

$$\vec{u}_{rel,coll} = \vec{u}_{rel}\left(\frac{r_1^3}{r_1^3 + r_2^3}\right). \tag{11}$$

The absolute velocity of the coalescence product droplet follows to be the vector sum of $\vec{v}_1$ and $\vec{u}_{rel,coll}$.

The velocities of the droplet main fractions after a stretching separation can be derived from a droplet kinetic energy balance. Using the simplified notation v instead of $\mid \vec{v} \mid$ for the absolute droplet velocity, the following results are obtained for the projected velocities of both droplets after separation (Fig. 10c)

$$v_{new1,proj} = \frac{v_2 r_2^3 + v_1 r_1^3 + r_2^3(v_1 - v_2)ZZ}{r_1^3 + r_2^3} \quad v_{new2,proj} = \frac{v_2 r_2^3 + v_1 r_1^3 - r_1^3(v_1 - v_2)ZZ}{r_1^3 + r_2^3}. \tag{12}$$

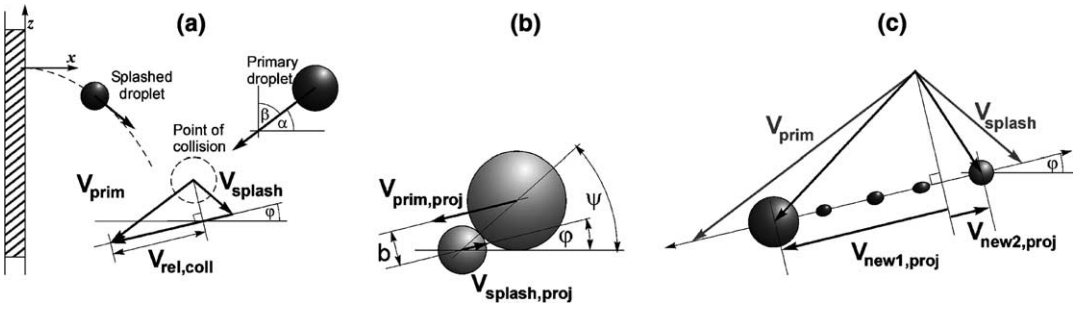

Fig. 10. Collision configuration of a splashed and representative primary spray droplet: (a) prior to collision, (b) at the moment of impact, (c) during the process of stretching separation.

The random variable ZZ is defined as $ZZ = (B - B_{cr})/(1 - B_{cr})$. Thereby, as can be seen in Fig. 10b the parameter B is related to the impact angle by the relation $B = \sin(\psi - \varphi)$. As follows from Eq. (12) the droplet fractions continue to move in the direction of motion of the droplet pair prior to impact with reduced velocity. The droplet components in the original coordinate frame can be reconstructed from the projected velocities according to the configuration given in Fig. 10.

The formation of satellite droplets results from the ligament stretching process during formation of the mean fragments, as investigated by Brenn et al. (2001) and by Georjon and Reitz (1999). After the ligament breakup the satellites arrange along the connecting line between the mean fragments. An estimation for the radius of the droplet fragments r_{child} is given by a correlation of Georjon and Reitz (1999), assuming equal sized fragmentation

$$r_{child} = \frac{1.89 r_{1+2}}{\sqrt{2.81\, We_{PA}^{2/7}(1+\gamma^3)^{2/21} + 1}}, \tag{13}$$

where their Weber number is defined as

$$We_{PA} = \rho u_{rel}^2 (r_1 + r_2)/\sigma \tag{14}$$

and r_{1+2} is the radius of a spherical droplet which would result from the stable coalescence of the collision partners.

4. Computation of deposition fractions

The objective of the simulation is to provide the properties of the droplets leaving the collision domain after encountering primary/secondary spray interaction and the wall deposition flux. The liquid fluxes for a given impingement configuration are determined in a Monte Carlo simulation. Characteristics of the primary and the secondary spray are represented by model droplet ensembles resembling the measured spray properties as an input for the calculation. The model droplet ensemble of the primary spray flux fits the measured free-stream size- and velocity distributions. The volume of the splashed droplets ejected in a single droplet splashing event is not easily accessible, due to the unknown amount of film liquid entrained. The splashing liquid flux emitted from the wall is approximately given from the overall liquid flux balance as the difference between primary spray feed stream and deposition flux. The model droplet ensemble of the secondary spray is also constructed from the measured spray, according to the experimental conditions under consideration; cf. Figs. 5, 6 and 8.

In principle the splashing droplets start velocity from the wall is difficult to evaluate due to the potential momentum interaction with the impinging primary spray. The secondary sprays measured data are assumed to represent essentially the non-colliding splashed droplet fraction, even in case of steep impact angle. This hypothesis can be confirmed by the calculated results, showing the collision product droplets preferentially to be transported towards the wall. Thereby the secondary spray data will be contaminated by collision effects only to a minor extent. The absolute velocity of the splashed droplets ejected from the wall is therefore estimated from the component velocity measurements given in Fig. 8.

4.1. Entrainment fraction

Following the arguments in Section 1, the entrainment fraction for the coarse primary spray was neglected in the calculations.

4.2. Splashing liquid fraction

With the underlying assumption that the splashed mass and the mass of the impacting droplet are identical, the amount of liquid rejected from the wall after impingement is determined solely from the splash criterion (2) with $K_{cr} = 138$, as suggested by the droplet impingement experiments on films of Cossali et al. (1997). It is important to note, that the lateral component of the primary spray droplet velocity has a considerable contribution to the droplet's wall normal velocity component and therefore on the K-number, especially in case of impingement with flat spray inclination against the wall. The lateral droplet velocity component from the experiments with the 0.7 bar spray has a mean value in the order of 1.0 m/s. It can be observed as a slight increase of the flat spray's depth in downstream direction.

4.3. Colliding fraction of the splashed liquid

The collision product flux, as the outcome of the collision events is a function of the splashing product flux, entering the domain Ω, where the splashed droplets ejected from the wall preferentially collide with droplets in the primary spray jet.

The colliding liquid volume flux $\dot{m}_{coll\_tot}$ was defined as the part of the splashed liquid flux $\dot{m}_{splash\_tot}$, which interacts in the form of collisions with the primary spray droplets. The relative colliding liquid fraction $\eta_{coll} = \dot{m}_{coll\_tot}/\dot{m}_{splash\_tot}$ can be calculated from (8) by inserting the expression for N_{coll} from (7). The droplet number concentration n_d in the primary spray jet is defined by

$$n_d = \frac{6\varepsilon_{prim}}{\pi(d_{30,prim})^3} \tag{15}$$

with the dispersed phase volume fraction ε_{prim} of the spray jet at nozzle distance L

$$\varepsilon_{prim} = \dot{m}_{prim}\rho/(\bar{v}_{ax,prim}A_{prim}). \tag{16}$$

In Eq. (15) $d_{30,prim}$ denotes the volume mean diameter of the primary spray. The number concentration n_d should represent the coarse droplet fraction, which is most relevant in the collision mechanism and therefore the median of the volume distribution was used to characterize the primary spray. For the quantity $\bar{v}_{ax,prim}$ an average of the droplet velocities, weighted per droplet mass, was used. A_{prim} is the primary spray's jet cross-section at the nozzle distance L from wall impact.

The residence time τ of the splashed droplet and its path length s within the interaction domain can be estimated from a trajectory calculation for the process of splashed droplet ejection from the wall. As an initial estimate the calculation of τ is performed for the simplified two-dimensional configuration shown in Fig. 11. The angle of ejection of the splashed droplet is denoted by θ_0, and its start velocity by $\bar{v}_0$. The local inclination of the trajectory from the horizontal is measured by ϕ. The droplet's gravity force is mg. The primary spray jet inclination angle from the horizon-

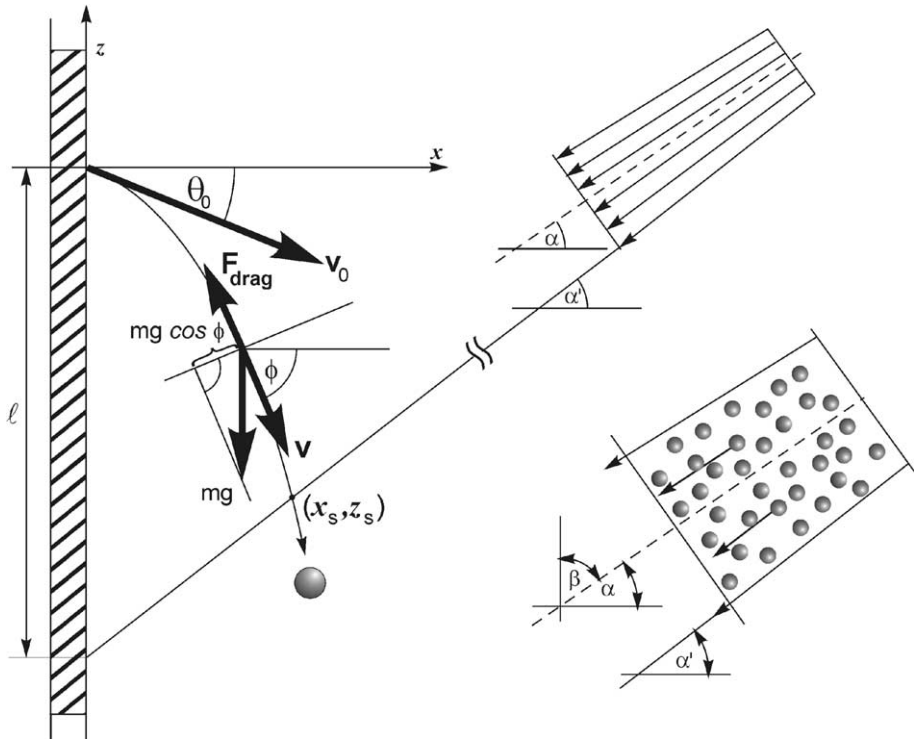

Fig. 11. Schematic of the lower jet boundary of the impinging primary spray and the splashed droplet trajectory in the wall coordinate system.

tal is denoted by α, and the corresponding angle of the lower spray jet boundary is α'. The penetration depth l is the vertical distance of the splashing droplet's start position measured from the lower bound of the primary spray jet. Parametric equations for the coordinate positions along the trajectory path, for the path length and the flight time can be derived from the droplet momentum balance in the wall normal direction x and in the direction normal to the path; see Eqs. (A.1) and (A.2) in Appendix A.

The intersection point of the trajectory with the lower spray jet boundary is (x_s, z_s), and the trajectory's angle of inclination at this point is ϕ_s. The coordinates (x_s, z_s) obey the relation

$$z_s = (\tan \alpha')x_s + l, \tag{17}$$

where z_s and x_s are given by extending the integration limits in Eqs. (A.3) from θ_0 to ϕ_s. Integration is performed by an adaptive, recursive Newton–Cotes rule until reaching the intersection, where Eq. (17) is satisfied. The residence time τ follows from the path length s of the flight to the intersection and the relation $\mathrm{d}s = v\,\mathrm{d}t$ in the form

$$\tau = -\int_{\theta_0}^{\phi_s} \frac{v}{g}\frac{1}{\cos\phi}\,\mathrm{d}\phi. \tag{18}$$

4.4. Collision outcome

As a consequence of collisions between splashed liquid and primary spray the processes of coalescence or stretching separation are considered. The corresponding mechanism for each simulated collision event is selected by comparison of the randomly selected droplet center displacement b with the critical displacement b_{cr} of Eq. (10). Following the direction of the flight of the droplets produced by the interaction, the total collision product flux can be divided into a fraction, which is directed towards the wall and a second fraction, which is able to escape the interaction domain.

The droplet diameter produced by the coalescence of the collision partners is calculated from the merged liquid volume. The corresponding velocity of the coalescence product droplet follows from Eq. (11). The diameter of the fragment droplets produced in the case of a stretching separation is estimated by Eq. (13) under the simplifying assumption of equal sized fragments. In principle this simplification can be improved by incorporation of a more sophisticated fragment size distribution, for example one based on the investigation of Brenn et al. (2001). However, this refinement is not implemented in the present calculations. The total number of fragments resulting in the stretching separation is given by

$$N_{\mathrm{frac}} = (r_{1+2}/r_{\mathrm{child}})^3 \tag{19}$$

with r_{child} as defined in Eq. (13). In the case where two fragments are predicted, their velocities are calculated by Eq. (12). If the number of fragments is greater than two, they are equally spaced along the connecting line between the original proposed mean fragment positions and their individual velocities are calculated according to the velocity vector diagram in Fig. 10c.

4.5. Balance of the liquid flux

The primary spray flux $\dot{m}_{\mathrm{prim}}$ is given by the nozzle feed stream. The balance of the liquid flux is closed by ignoring the transfer of preexisting film liquid into droplets during the splashing process. Under this assumption the remaining unknown fluxes are defined by the set of balance equations, which is formally stated by the linear system

$$\begin{pmatrix}
1 & 0 & 0 & 0 & 0 & 0 & 0 & 0 & 0 & 0 \\
0 & 1 & 0 & 0 & 0 & 0 & 0 & 0 & 0 & 0 \\
0 & 0 & 1 & 0 & 0 & 0 & 0 & 0 & 0 & 0 \\
0 & 0 & -1 & 1 & 0 & 0 & 0 & 0 & 0 & -1 \\
0 & 0 & 0 & -\eta_{\mathrm{coll}} & 1 & 0 & 0 & 0 & 0 & 0 \\
0 & 0 & 0 & -(1-\eta_{\mathrm{coll}}) & 0 & 1 & 0 & 0 & 0 & 0 \\
0 & 0 & 0 & 0 & -\eta_{\mathrm{walldir}} & 0 & 1 & 0 & 0 & 0 \\
0 & 0 & 0 & 0 & -(1-\eta_{\mathrm{walldir}}) & 0 & 0 & 1 & 0 & 0 \\
0 & 0 & 0 & 0 & 0 & 0 & -(1-\eta_{\mathrm{splash}}) & 0 & 1 & 0 \\
0 & 0 & 0 & 0 & 0 & 0 & -\eta_{\mathrm{splash}} & 0 & 0 & 1
\end{pmatrix} \dot{\mathbf{m}}$$

$$= \begin{pmatrix} 0 \\ (1-\eta_{\text{splash}})\dot{m}_{\text{prim}} \\ \eta_{\text{splash}}\dot{m}_{\text{prim}} \\ 0 \\ 0 \\ 0 \\ 0 \\ 0 \\ 0 \\ 0 \end{pmatrix} \tag{20}$$

with the vector of the fluxes $\dot{\mathbf{m}} = col(\dot{m}_{\text{prim\_entrain}}, \dot{m}_{\text{prim\_dep}}, \dot{m}_{\text{prim\_splash}}, \dot{m}_{\text{splash\_tot}}, \dot{m}_{\text{coll\_tot}}, \dot{m}_{\text{splash+escape}}, \dot{m}_{\text{coll\_walldir}}, \dot{m}_{\text{coll\_envdir}}, \dot{m}_{\text{coll+dep}}, \dot{m}_{\text{sec\_splash}})$. The series of the liquid fluxes in $\dot{\mathbf{m}}$ is defined as follows: the flux of droplets directly entrained in the wall-jet $\dot{m}_{\text{prim\_entrain}}$, the flux of the primary spray directly deposited on the wall $\dot{m}_{\text{prim\_dep}}$, the flux of the primary spray splashed directly during the impingement $\dot{m}_{\text{prim\_splash}}$, the total flux of the liquid produced by splashing, which is $\dot{m}_{\text{splash\_tot}} = \dot{m}_{\text{prim\_splash}} + \dot{m}_{\text{sec\_splash}}$, the liquid flux participating in the collision process $\dot{m}_{\text{coll\_tot}}$, the flux of the splashed liquid leaving the interaction domain $\dot{m}_{\text{splash+escape}}$, the wall-directed and freestream-directed fluxes of the collision products $\dot{m}_{\text{coll\_walldir}}$ and $\dot{m}_{\text{coll\_envdir}}$, the depositing and the splashing liquid fluxes from the wall-directed stream of collision products $\dot{m}_{\text{coll+dep}}$ and $\dot{m}_{\text{sec\_splash}}$. The partitioning of the fluxes is determined by the three splitting fractions η_{splash}, η_{coll} and η_{walldir}. The deposition fraction η_{coll} is calculated from Eq. (8). The wall-directed fraction η_{walldir} of the collision droplets is calculated by a Monte Carlo simulation of the collision outcome based on Eqs. (9)–(14).

4.6. Simulation results

Sample results will be discussed for the case with a wall film and a nozzle feed pressure of 0.7 bar. As calculation input for the spray interaction, experimental secondary spray data was selected as follows. The splash droplet's arithmetic mean diameter was chosen as $d_{10,\text{splash}} = 0.85 d_{10,\text{prim}}$, according to the data in Fig. 5, where it was shown to be nearly independent from the primary spray impact angle. The secondary spray's droplet spectrum covering a droplet size range within $50 < d_{\text{sec}} < 1300\,\mu\text{m}$, according to Fig. 6, was fitted by the distribution function (1). As a consequence of the uncertainty introduced by the potential influence of droplet interaction, as a rough estimate an average value of $\bar{v}_{\text{sec}} = 4\,\text{m/s}$, independent of the impingement angle, was used as the calculation-input for the secondary droplet wall ejection velocity. This choice is also supported by the data of Reske (1987), who performed single droplet splash experiments against moving liquid films with primary droplets in the order of millimeters.

Results show that the directly deposited fraction of the primary spray $\dot{m}_{\text{prim\_dep}}$ is in the order of 50% for flat impingement angles ($\beta = 15°$) and approaches zero for steep impingement angles.

The τ-distribution for different primary spray impingement angles is shown in Fig. 12. The splashed droplets residence times in the interaction domain are found to be in the millisecond

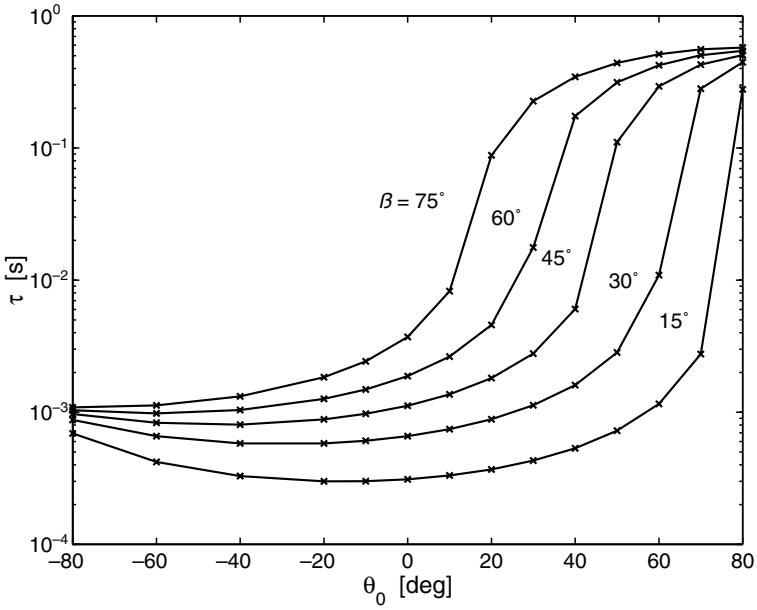

Fig. 12. Residence time τ of splashed droplets in the primary/secondary spray interaction domain for different primary spray impingement angles; ejection pressure $\Delta p = 0.7$ bar.

range for the dominating fraction of the downward directed splash droplets and may reach the order of some hundred milliseconds for the rare case of upward injected splash droplets. A length $l = 5$ mm was set as a mean value for the distance of a characteristic splash position to the primary jet boundary. The colliding liquid fraction of the splashing flux η_{coll} was calculated for the experimental impingement primary spray cross-section of 0.12×0.02 m. Even in the case of flat spray impingement against the wall, nearly 50% of the splashing liquid encounters collisions with the primary spray and for steep impingement the colliding fraction exceeds 90%; see Fig. 13.

The size of the droplet fragments after stretching separation as calculated from Eq. (13) is shown in Fig. 14. Note that the definition of the *We*-number in the plot is according to Eq. (14). The droplets in the simulation cover the range $100 < We_{\mathrm{PA}} < 1000$. As a comparison, the fragment size prediction of Dohmann (1998) from an experimental investigation of droplet collisions in intersecting spray cones is also included in Fig. 14. Dohmann's experimental data forms a lower bound of possible droplet size decrease for the case of high-*We*-number impacts in overlapping sprays. Note however, that typical impact angles ψ in the simulation are smaller than Dohmann's spray impact angle of $\psi = 120°$.

The collision product flux is split into wall-directed and freestream-directed fractions according to the velocities of the droplets produced by coalescence and stretching separation. The simulation demonstrates that the majority of the collision product flux is directed towards the wall. The wall-directed droplets are confronted by the splash criterion Eq. (2) like the impinging primary spray droplets. The simulation reveals that wall-directed droplets formed by coalescence typically splash, whereas smaller stretching separation fragments approaching the wall typically undergo deposition. The deposition fraction of the collision product flux decreases with increasing

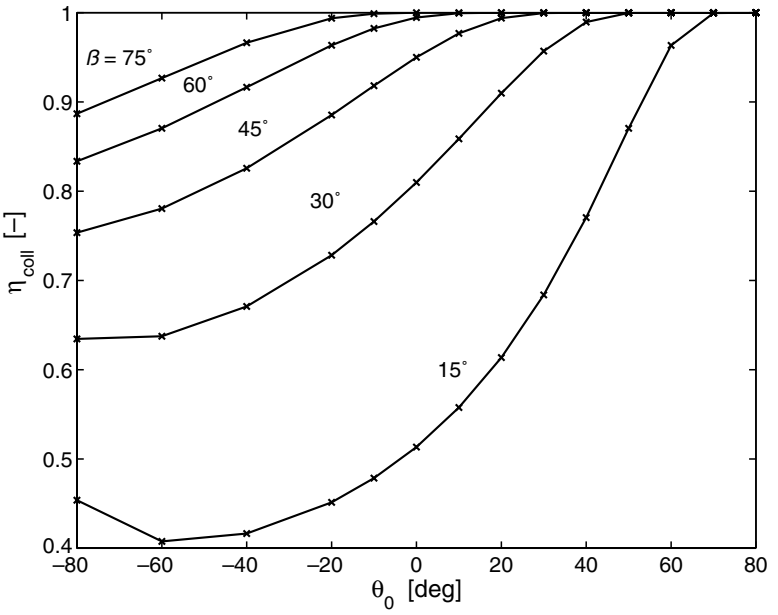

Fig. 13. Colliding liquid fraction in the splashed liquid flux; ejection pressure $\Delta p = 0.7\,\text{bar}$, $d_{30,\text{prim}} = 1000\,\mu\text{m}$, $d_{30,\text{splash}} = 800\,\mu\text{m}$, $\bar{v}_{\text{prim}}(d_{30}) = 7.4\,\text{m/s}$, $\bar{v}_{\text{splashed}} = 4.0\,\text{m/s}$.

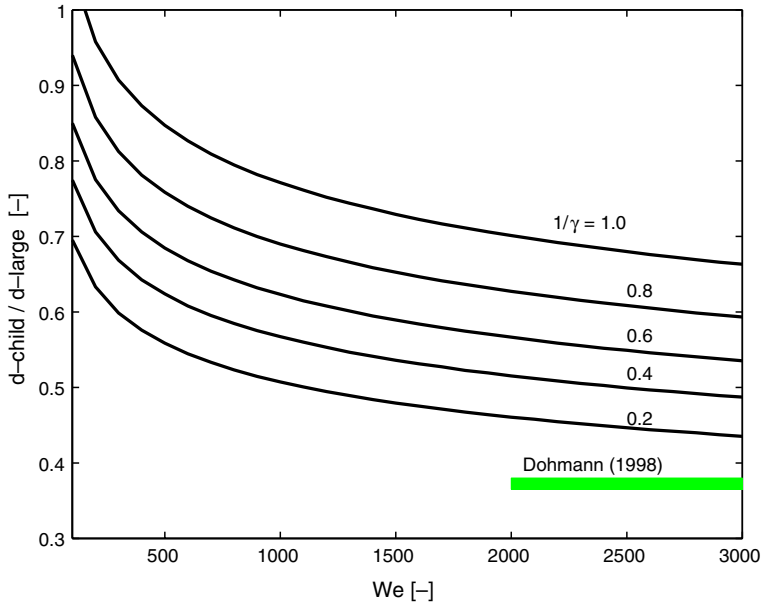

Fig. 14. Droplet diameters of the fragments from collisions followed by stretching separation; colliding droplet diameter ratio $1/\gamma$ as a parameter.

impingement angle β (Fig. 15) and does not show a significant dependence on the splashed droplet's ejection angle θ_0. Following from the overall liquid balance, the partial deposition of the wall-directed collision product flux turns out to be the dominating deposition mechanism.

The freestream-directed collision product droplets leave the interaction domain preferentially at flat angles from the wall; see Fig. 16. These findings are roughly consistent with the experimentally

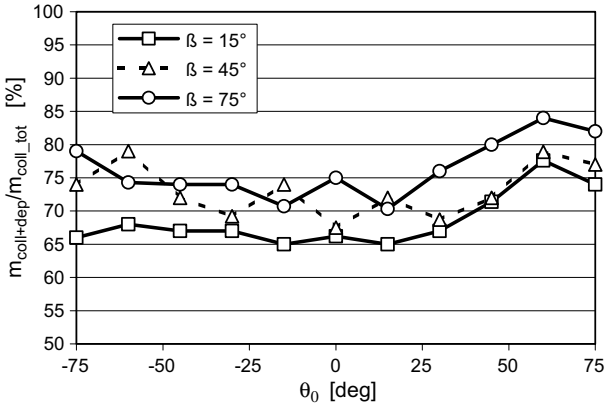

Fig. 15. Deposition fraction of the collision product droplet flux.

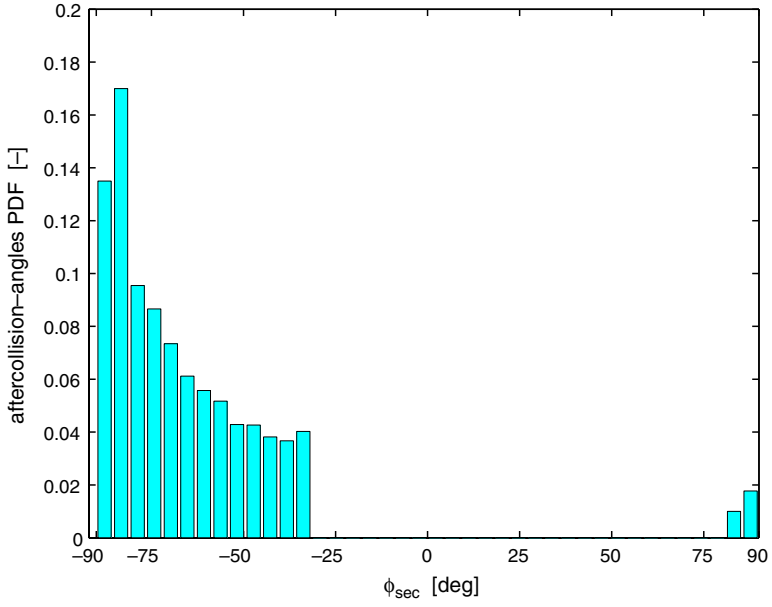

Fig. 16. Probability distribution of inclination angles ϕ_{sec} predicted for the collision product droplets; simulation with $\beta = 15°$, $\bar{v}_{prim} = 10\,m/s$, $\theta_0 = -45°$, $v_0 = 4.0\,m/s$.

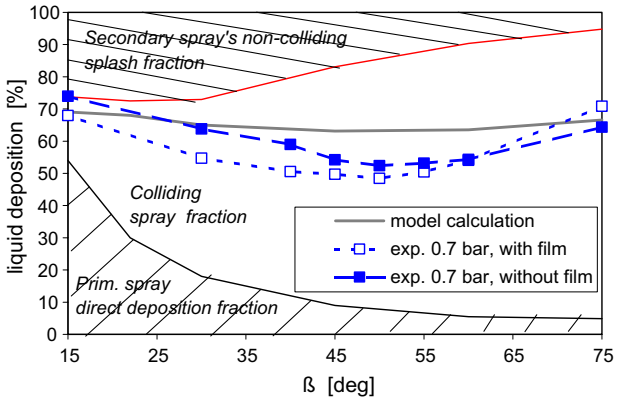

Fig. 17. Measured and simulated total liquid deposition fraction as a function of the impingement angle; 0.7 bar experiment.

detected mean values of the secondary droplet trajectory inclination angles ϕ_{sec}, which were determined to be in the range of $6° < |90 - \phi_{sec}| < 12°$; (according to the definition of the secondary droplet angle ϕ in Fig. 11).

At $\beta = 45°$ the colliding liquid flux turns out to be even larger than the primary spray's splashing liquid fraction. Due to the high amount of large droplets formed by coalescence, a considerable amount of the wall-directed collision product flux undergoes splashing and thereby the liquid becomes partially trapped within the interaction zone.

A comparison of measured and simulated liquid deposition fractions as a function of the primary spray's impingement angle is shown in Fig. 17. The preliminary model predicts quantitatively the order of magnitude of the deposition fraction and at least shows the correct trend within the collision dominated regime at steep impingement angles. The calculated minimum of the deposition curve is relatively flat and not so distinct, as compared to the experiments. The total liquid deposition is overpredicted by roughly 10–15% in the intermediate range of impingement angles.

5. Summary and conclusions

The wall impingement of coarse sprays with a mean diameter d_{10} in the order of millimeters was investigated experimentally and theoretically to identify the physical mechanisms of liquid deposition on the wall. In impingement experiments with a flat fan spray the liquid deposited on the wall was measured as a function of the primary spray impingement angle. The secondary spray's droplet size and velocity distributions were characterized by phase Doppler measurements at a distance of 150 mm and 450 mm below the impact location, to ensure a relaxation of possible droplet deformations, which might accompany the splash process. The size distribution of the secondary spray was found to be even narrower than that of the primary spray. The liquid deposition fraction turned out to be up to one order of magnitude higher than the value predicted by single droplet based deposition-splash criteria.

The experiment revealed that the splashed droplets hit the primary spray in a cross-stream configuration after their ejection from the wall. Therefore, inter-droplet collisions between splashed and primary spray droplets are postulated to play an important role in the impingement dynamics. The range of steep impingement configuration produces, what was termed an "enhanced droplet interaction regime".

Collision rates were estimated based on typical splashed droplet residence times within the interaction domain of the primary spray jet. The collision outcome was simulated by a Monte Carlo procedure, taking into account droplet coalescence and secondary breakup due to stretching separations. As a result of the enhanced droplet interaction regime, the predictions show that the liquid deposition on the wall is mainly caused by wall-directed collision product droplets. Comparing the calculations with the experimentally determined deposition fractions the model shows the correct trend with a flat minimum of the deposition, which is predicted in the intermediate range of impingement angles. At the location of the minimum the deposition is overestimated in the simulation by approximately 15%. Although the model outcome in principle could be fine-tuned by relaxing the assumption of uniform splashing droplets' starting velocity and starting position in the impingement spray's jet cross-section, so far no attempt was undertaken in this direction. Impinging spray simulations, in principle, might contribute to a more in-depth analysis of the near wall region's spray interaction mechanism.

Acknowledgment

The experimental section of this work was supported by the Austrian Science Foundation ("Fonds zur Förderung der wissenschaftlichen Forschung") under FWF project number P-15245. The author gratefully acknowledges this support and would like to thank Ulrich Wieltsch and Martin Dopler for performing the measurement series.

Appendix A

Simplified description of the splashed droplet trajectories.

The primary spray induced gas motion forms a wall-jet configuration with a stagnation region, which is centered at the intersection of the primary spray's jet axis with respect to the wall. The gas velocity is expected to be small in the stagnation region, justifying $\vec{w}_g = 0$ as a simplification within Ω. As a consequence, the splashed droplets' trajectory calculation can be based on the derivation of Allen (1988), which is used in the present investigation to develop explicit integral expressions for the droplets' path length and the droplet residence time within the interaction domain. With the definition of ϕ as the angle between the droplet absolute velocity $\vec{v}$ and the x-axis, the droplet momentum equation in the x-direction can be stated for the special case of $\vec{w}_g = 0$ in the form

$$m\frac{d^2x}{dt^2} = -|\vec{F}_{drag}|\cos\phi \tag{A.1}$$

with $\vec{F}_{\mathrm{drag}} = 0.5 c_{\mathrm{D}} \rho_{\mathrm{g}} A \mid \vec{v}_{\mathrm{r}} \mid \vec{v}_{\mathrm{r}}$. Therein the notation of Fig. 11 is applied with the origin of the wall coordinate system defined in the position of the droplet's splash center. The symbols c_{D}, ρ_{g}, A, $\vec{v}_{\mathrm{r}}$ denote the drag coefficient, the gas density, the droplet's cross-sectional area and the relative velocity between the droplet and the gas phase $\vec{v}_{\mathrm{r}} = \vec{v} - \vec{w}_{\mathrm{g}}$, which under the simplification $\vec{w}_{\mathrm{g}} \approx 0$ reduces to $\vec{v}_{\mathrm{r}} \approx \vec{v}$. The momentum equation in the direction normal to the path at any point on the trajectory (with the absolute length v of the instantaneous droplet velocity vector) gives

$$v^2/r = g \cos\phi \tag{A.2}$$

as an expression for the acceleration in the normal direction of the droplet motion.

Following the derivation of Allen (1988) and again making use of the simplification $\vec{v}_{\mathrm{r}} \approx \vec{v}$, the wall normal and tangential coordinates along the splashing droplet trajectory can be derived from the momentum equations (A.1) and (A.2) in the form

$$x = -\int_{\theta_0}^{\phi} \frac{v^2}{g}\,\mathrm{d}\phi \quad \text{and} \quad z = -\int_{\theta_0}^{\phi} \frac{v^2}{g} \tan\phi\,\mathrm{d}\phi, \tag{A.3}$$

where the term v^2/g in the integral is given (with the abbreviation $c = 0.5 c_{\mathrm{D}} \rho_{\mathrm{g}}$it A/$m$ and c_{D} kept constant) by the expression

$$\frac{v^2}{g} = \left(\frac{v_0^2}{g \sec^2\theta_0 - 2 c v_0^2 [\xi(\phi) - \xi(\theta_0)]} \right) \frac{1}{\cos^2\phi} \tag{A.4}$$

with the function $\xi(k)$ defined slightly differently but equivalent to Allen's form, as

$$\xi(k) = \frac{1}{2}\left[\frac{\sin k}{\cos^2 k} + \frac{1}{2} \ln \left| \tan\left(\frac{k}{2} + \frac{\pi}{4} \right) \right| \right].$$

In the trajectory calculation the integrations in (A.3) and in Eq. (18) are performed stepwise, while updating the drag coefficient according to the correlation $c_{\mathrm{D}} = 24\, Re^{-1} + 0.1\, Re^{-0.5} + 0.4$ for every angle increment $\mathrm{d}\phi$.

References

Allen, R.F., 1988. The mechanics of splashing. J. Coll. Interface Sci. 124, 309–316.

Amsden, A.A., O'Rourke, P.J., Butler, T.D., 1989. KIVA-II: a computer program for chemically reactive flows with sprays. Los Alamos National Laboratory Report LA-11560-MS.

Ashgriz, N., Poo, J.Y., 1990. Coalescence and separation in binary collisions of liquid drops. J. Fluid Mech. 221, 183–204.

Blei, S., Sommerfeld, M., 2002. Experimentelle Untersuchung von Tropfenkollisionen als Basis lagrangscher Modellierungen. Spray, Freiberg (Germany).

Brazier-Smith, P., Jennings, S., Latham, J., 1972. The interaction of falling rain drops: coalescence. Proc. Royal Soc. Lond. A 326, 393–408.

Brenn, G., Durst, F., Zambotti, S., 1996. Experimental investigations on multiple spray interaction with solid walls. Entropie 200, 29–36.

Brenn, G., Kalenderski, S., Ivanov, I., 1997. Investigation of the stochastic collisions of drops produced by Rayleigh breakup of two laminar liquid jets. Phys. Fluids 9, 349–364.

Brenn, G., Valkovska, D., Danov, K.D., 2001. The formation of satellite droplets by unstable binary drop collisions. Phys. Fluids 13, 2463–2477.

Briffa, F.E.J., Dombrowski, N., 1966. Entrainment of air into a liquid spray. AIChE J. 12, 708–717.

Coghe, A., Cossali, G.E., Marengo, M., 1995. A first study about single drop impingement on thin liquid film in a low Laplace number range. Proceedings of PARTEC'95, Nürnberg.

Cossali, G.E., Coghe, A., Marengo, M., 1997. The impact of a single drop on a wetted surface. Exp. Fluids 22, 463–472.

Dohmann, J., 1998. Sekundärdispersion und Koagulation von Tropfen in sich überschneidenden Sprays. Chem. Ing. Tech. 70, 534–538.

Estrade, J.P., Carentz, H., Lavergne, G., Biscos, Y., 1999. Experimental investigation of dynamic binary collision of ethanol droplets—a model for droplet coalescence and bouncing. Int. J. Heat Fluid Flow 20, 486–491.

Gavaises, M., Theodorakakos, A., Bergeles, G., Brenn, G., 1996. Evaluation of the effect of droplet collisions on spray mixing. Proc. Inst. Mech. Engrs. 210, 465–475.

Georjon, T.L., Reitz, R.D., 1999. Drop-shattering collision model for multidimensional spray computations. Atomization Sprays 9, 231–254.

Macklin, W.C., Metaxas, G.J., 1976. Splashing of drops on liquid layers. J. Appl. Phys. 47, 3963–3970.

Marple, V.A., Liu, Y.H., 1974. Characteristics of laminar jet impactors. Env. Sci. Technol. 8, 648–654.

Mohammadi, A., Miwa, K., Kidoguchi, Y., 2000 High time-space resolution analysis of droplets behaviour and gas entrainment into diesel sprays impinging on a wall. Proceedings of ILASS-Europe 2000, Darmstadt (Germany), VII.5.1–5.6.

Mundo, C., Sommerfeld, M., Tropea, C., 1995. Droplet-wall collisions: experimental studies of the deformation and breakup process. Int. J. Multiphase Flow 21, 151–173.

O'Rourke, P.J., Amsden, A.A., 2000. A spray/wall interaction submodel for the KIVA-3 wall film model. Soc. Automot. Engng., 2000-01-0271.

O'Rourke, P.J., Bracco, F., 1980. Modeling of drop interactions in thick sprays and a comparison with experiments. Proc. Inst. Mech. Engrs. 9, 101–106.

Post, S.L., Abraham, J., 2002. Modeling the outcome of drop-drop collisions in Diesel sprays. Int. J. Multiphase Flow 28, 997–1019.

Prosperetti, A., Oguz, H.N., 1993. The impact of drops on liquid surfaces and the underwater noise of rain. Ann. Rev. Fluid Mech. 25, 577–602.

Rein, M., 1993. Phenomena of liquid drop impact on solid and liquid surfaces. Fluid Dyn. Res. 12, 61–93.

Reske, R., 1987. Experimentelle Untersuchung des Verhaltens frei fallender Wassertropfen beim Auftreffen auf dünnen Wasserfilm. Fortschr.-Ber. VDI Reihe 7; Nr. 115.

Samenfink, W., Elsäßer, A., Dullenkopf, K., Wittig, S. 1997 Droplet interaction with shear-driven liquid films: high quality measurements of the deposited mass fraction. Proceedings of ILASS-Europe'97; Florenz (Italy), pp. 480–486.

Tropea C. 1999. Spray modelling and its experimental verification. AVL CFD User Meeting'99; Graz (Austria), pp. 1–15.

Tropea, C., Roisman, I.V., 2001. Modeling of spray impact on solid surfaces.. Atomization Sprays 10, 387–408.

Walzel, P., 1980. Zerteilgrenze beim Tropfenaufprall. Chem. Ing. Tech. 52, 338–339.

Wieltsch, U., Dopler, M., Weiss, C., Marr, R., 1998. Investigation on the development of the wall film in scrubbers. Proceedings of ILASS-Europe'98, Manchester (Great Britain), pp. 445–450.

Yarin, A.L., Weiss, D.A., 1995. Impact of drops on solid surfaces: self-similar capillary waves and splashing as a new type of kinematic discontinuity. J. Fluid Mech. 283, 141–173.